



# Monomeric cohesin state revealed by live-cell single-molecule spectroscopy

Wenjie Liu<sup>1,2,†</sup>, Elisheva Biton<sup>3,†</sup>, Anjali Pathania<sup>3</sup>, Avi Matityahu<sup>3</sup>, Joseph Irudayaraj<sup>1,2,\*</sup>  & Itay Onn<sup>3,\*\*</sup> 

## Abstract

The cohesin complex plays an important role in the maintenance of genome stability. Cohesin is composed of four core subunits and a set of regulatory subunits that interact with the core subunits. Less is known about cohesin dynamics in live cells and on the contribution of individual subunits to the overall complex. Understanding the tethering mechanism of cohesin is still a challenge, especially because the proposed mechanisms are still not conclusive. Models proposed to describe tethering depend on either the monomeric cohesin ring or a cohesin dimer. Here, we investigate the role of cohesin dynamics and stoichiometry in live yeast cells at single-molecule resolution. We explore the effect of regulatory subunit deletion on cohesin mobility and found that depletion of different regulatory subunits has opposing effects. Finally, we show that cohesin exists mostly as a canonical monomer throughout the cell cycle, and its monomeric form is independent of its regulatory factors. Our results demonstrate that single-molecule tools have the potential to provide new insights into the cohesin mechanism of action in live cells.

**Keywords** chromosome; cohesin; fluorescence correlation spectroscopy; photon counting histogram; SMC complexes

**Subject Categories** Cell Cycle; Structural Biology

**DOI** 10.15252/embr.201948211 | Received 2 April 2019 | Revised 28 November 2019 | Accepted 4 December 2019 | Published online 29 December 2019

**EMBO Reports (2020) 21: e48211**

## Introduction

The structural maintenance of chromosome (SMC) complex, cohesin, is involved in the higher-order organization of chromatin in the cell nucleus. During cell cycle, cohesin holds the newly formed sister chromatids from the time of their formation at the S phase of the cell cycle until their separation in mitosis. This process, known as sister chromatid cohesion, ensures the bipolar attachment of the centromeres to the spindle and, in turn, the accurate segregation of the chromatids during cell division [1–4].

The core cohesin complex is a ring composed of Smc1, Smc3, and Scc1/Mcd1/Rad21 [5]. The proteins Scc3, Pds5, and Wpl1 form a regulatory subcomplex that binds cohesin through Scc1 [5–10]. In *Saccharomyces cerevisiae*, the cohesin complex assembly is regulated by Scc1, which is cleaved and degraded during anaphase and re-expressed in the late G1 stage of the following cell cycle [11,12]. Cohesin loading onto the chromatin starts at late G1 and continues during the S phase of the cell cycle [5,13]. At this stage, Wpl1 is thought to act as an antagonist that dissociates cohesin from the chromatin [6,8,14,15]. Following DNA replication, the chromatin-bound cohesin is transformed into the cohesive state that tethers two chromatin fibers [16–18]. Pds5 maintains cohesion during the G2 phase of the cell cycle by protecting cohesin from premature dissociation from the chromatin [7,19]. When cells enter mitosis, cohesin is removed from the chromatin by proteolytic cleavage of Scc1 by separase [11,20].

While the overall activity cycle has been described, previous studies, to a great extent, provide snapshots of the effect of the individual subunits on cohesin dynamics. Furthermore, the mechanism by which cohesin tethers chromatin remains controversial. Several biochemical studies suggest that the cohesin active unit is monomeric [21–23], while genetic evidence suggests that the cohesive form of cohesin contains cohesin dimers or multimers [24–28]. We will utilize single-molecule spectroscopy tools to discern cohesin binding mechanisms in live cells.

Advanced single-molecule spectroscopy tools such as fluorescence correlation spectroscopy (FCS) can facilitate the exploration of cohesin interaction in live cells. FCS is based on the correlation of fluctuations in fluorescence intensity as molecules diffuse through a sub-femtoliter volume (Fig 1A). This highly sensitive technique can provide information on real-time diffusion and interactions at single-molecule sensitivity. In cells, intermolecular interactions such as the formation of a cohesin–chromatin complex or major conformational changes can affect the diffusion rate (Fig 1B). Photon counting histogram (PCH) analysis of the fluorescence fluctuation signal enables stoichiometric analysis in live cells and the determination of the stoichiometry of target molecules (Fig 1C). In this work, utilizing single-molecule spectroscopy and analysis tools we

1 Department of Bioengineering, Micro and Nanotechnology Laboratory, Cancer Center at Illinois, University of Illinois at Urbana-Champaign, Urbana, IL, USA

2 Mills Breast Cancer Institute, Carle Foundation Hospital, Urbana, IL, USA

3 The Azrieli Faculty of Medicine, Bar-Ilan University, Safed, Israel

\*Corresponding author. Tel: +1 217 300 0525; E-mail: jirudaya@illinois.edu

\*\*Corresponding author. Tel: +972 72 2644 983; E-mail: itay.onn@biu.ac.il

†These authors contributed equally to this work

examine the effects of Pds5, Wpl1, and Eco1 on cohesin dynamics and their stoichiometry in live yeast cells. We expect our findings to provide new insights on cohesin dynamics in live cells.

## Results and Discussion

### Cell cycle-dependent molecular diffusion of cohesin complexes

To assess cohesin dynamics in live cells and the contribution of the individual subunits to the complex dynamics, we performed a series

of FCS analyses on several strains. The apparent diffusion time of cohesin subunits may be altered by conformational changes (for example, an elongated versus a folded SMC protein, an open versus a closed/folded ring), interaction with other molecules (protein–DNA or protein–protein interactions), and molecular crowding (e.g., chromosome condensation [29,30]). First, we evaluated the diffusion characteristics of Smc3-GFP throughout the cell cycle. Cells of strain  $\gamma$ AM085 (SMC3-GFP) were grown to mid-log phase and analyzed by FCS at different stages of the cell cycle. The phases were determined by cell morphology as described in the Materials and Methods section (Fig EV1). Typical fluorescence intensity trace

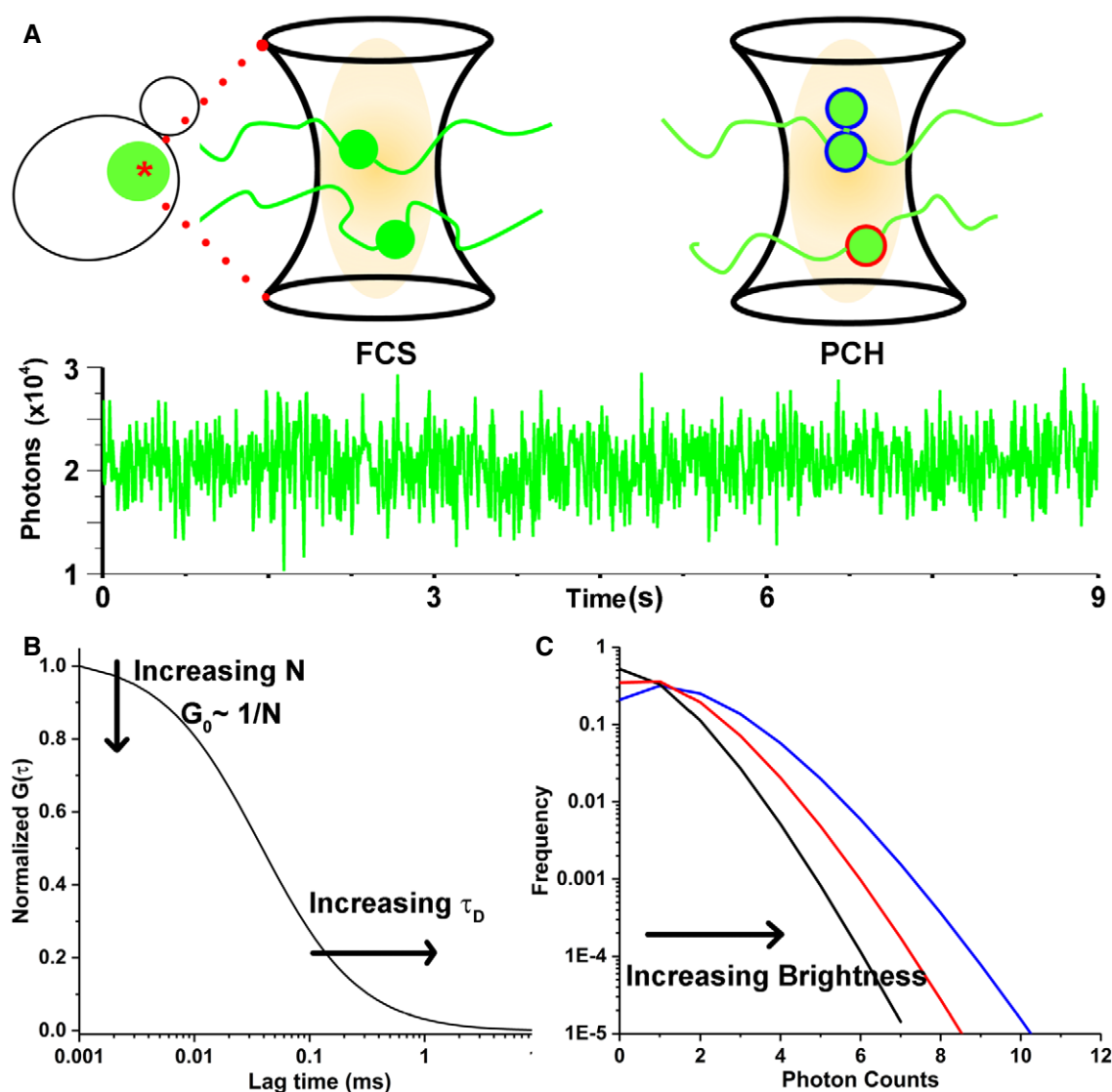


**Figure 1. Schematic of FCS and PCH analysis based on fluorescence intensity fluctuation.**

A One-color fluorescence autocorrelation spectroscopy (FCS) and photon counting histogram (PCH) are methods based on fluorescence fluctuation analysis of fluorescence intensity detected at a sub-femtoliter volume.

B FCS analysis yields a fluorescence autocorrelation function ( $G(\tau)$ ), which reports the average number of fluorescence molecules,  $N$  ( $N$  is inversely proportional to the correlation function amplitude  $G(0)$ ), and the mobility parameter of the molecules diffusing through the diffraction-limited volume ( $\tau_D$  is the translational diffusion time, and  $D$  is the diffusion coefficient). Faster mobility correlates with smaller  $\tau_D$ .

C PCH analysis is a reporter for the oligomerization state of fluorescence proteins. It reports the measured photon counts per molecule and the average number of molecules within the observation volume. Diagram illustrates potential oligomerization state of monomer (black), dimer (red), and trimer (blue) from PCH analysis.

was collected over 10 s, and the apparent transient diffusion time was fitted using the 3D one-component anomalous diffusion model (Fig 2A). Typical normalized FCS curves of Smc3-GFP at different phases of the cell cycle are shown (Fig 2B). In unbudded cells (G1), the diffusion time of Smc3-GFP was ~11.25 ms (Table 1, Figs 2C–F and EV2A). The diffusion time of Smc3-GFP increased to ~6.64 ms in cells with a small bud (S), indicating faster mobility of the protein. In G2 phase, the diffusion time decreased to ~8.49 ms, and in mitotic cells with dividing nuclei, the diffusion time of Smc3-GFP further decreased to ~13.3 ms, similar to the diffusion time of the protein at G1. Similar diffusion times were noted in cells with either Scc3-GFP or Scc1-GFP at G1 (only Scc3), S, and G2 phases.

However, at M phase, the diffusion times of Scc3 and Scc1 increased to 3.44 and 3.12 ms, respectively, suggesting faster mobility of the proteins and possibly a more freely diffused form (Table 1 and Figs 2C–F and EV2A). As expected, Scc1-GFP was not detectable in the cells at the G1 phase, since SCC1 expression starts in the late G1/S phase of the cell cycle [5,13].

Given that the molecular diffusion is negatively proportional to the hydrodynamic radius by Stokes–Einstein relation, our observation of the cohesin is in agreement with current models of the cohesin activity cycle and structural changes. During the S/G2 phase, Scc1/Scc3/Smc3 shows similar mobility that indicates the assembly of the subunits into the holocomplex that is loaded onto

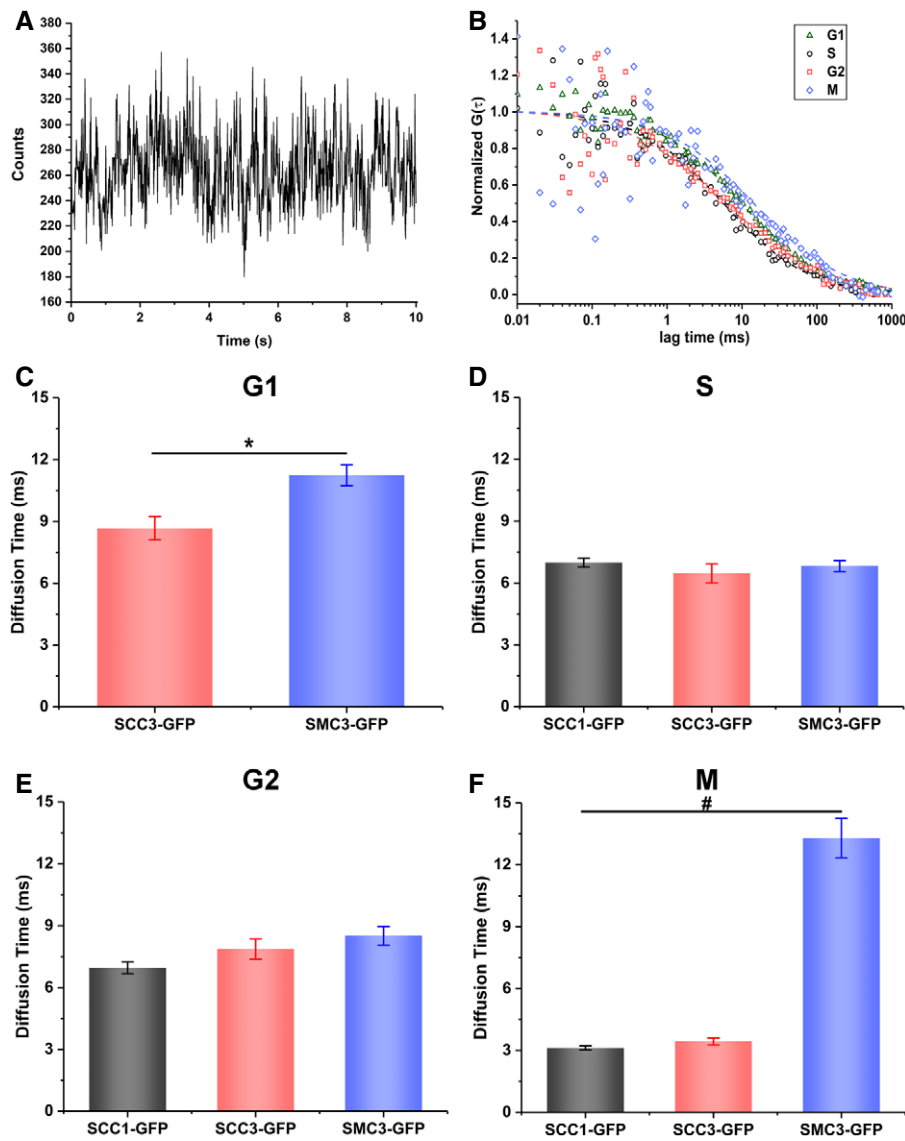


**Figure 2. Diffusion of cohesin subunits throughout the cell cycle.**

A Typical fluorescence intensity trace collected over 10 s.

B Typical normalized FCS curves of Smc3-GFP at different cell cycle phases. Dotted lines indicate fitting of the one-component anomalous diffusion model to the respective FCS curve.

C–F Diffusion times of Smc3-GFP, Scc3-GFP, and Scc1-GFP at the G1 phase (C), S phase (D), G2 phase (E), and mitosis (F). Data are shown as mean  $\pm$  SEM from at least three independent experiments. \* $P < 0.01$ ; # $P < 10^{-13}$  with the Mann–Whitney test.

**Table 1. Summary of cohesin holocomplex and subunit-depleted complexes on diffusion times throughout the cell cycle.**

Strain	Diffusion time in millisecond (n)			
	G1	S	G2	M
Smc3-GFP	11.24 ± 0.50 (75)	6.64 ± 0.22 (59)	8.49 ± 0.53 (47)	13.30 ± 0.95 (42)
Scs3-GFP	8.66 ± 0.57 (40)	6.47 ± 0.47 (23)	7.87 ± 0.49 (48)	3.44 ± 0.17 (40)
Scs1-GFP	N/A	6.99 ± 0.22 (87)	6.95 ± 0.29 (55)	3.12 ± 0.10 (86)
Scs1-GFP WPL1Δ	N/A	13.52 ± 0.59 (64)	7.18 ± 0.37 (38)	11.1 ± 0.47 (41)
Scs1-GFP Pds5-AID	N/A	4.31 ± 0.27 (38)	4.48 ± 0.37 (39)	2.34 ± 0.18 (18)
Scs1-GFP Scs3-AID	N/A	16.43 ± 0.80 (33)	16.76 ± 0.66 (46)	14.66 ± 1.59 (27)
Scs1-GFP Eco1-AID	N/A	15.23 ± 1.50 (27)	21.56 ± 1.70 (25)	9.20 ± 0.92 (27)

Data is shown as mean ± SEM from at least three independent experiments.

the chromatin, which, in turn, slows down its diffusion. As cells enter M phase, mobility of Scs1-GFP and Scs3-GFP increases. This observation is explained by cohesin dissociation from the chromatin and Scs1 cleavage by Esp1/separase [5,13]. The faster mobility of Scs1-GFP in M phase could be explained by a more freely diffused form of Scs1-GFP indicated by a 2-component FCS fit, as well as the increased free diffusion fraction of Scs1-GFP compared to S/G2 phase (Appendix Table S1). Scs3-GFP at M phase shows faster mobility, indicating the likelihood of a detached form of the protein. At the same stage, Smc3-GFP shows slower mobility, although Smc3 and Scs3 have a similar molecular mass. This result could be explained by a conformational change in Smc3 from a compact structure into an elongated form, as previously observed for soluble SMC proteins [31]. The possibility of a cleaved Scs1 N-terminus being bound to Smc3 decreasing its diffusion also exists.

#### The effect of regulatory subunit depletion of cohesin dynamics

Next, we explored the effect of the cohesin regulatory subunits Scs3, Wpl1, Pds5, and Eco1 on cohesin dynamics. For this purpose, we constructed a strain yEB005 in which Scs1 was fused to GFP, and WPL1 was deleted (SCS1-GFP WPL1Δ). We also constructed three additional SCS1-GFP strains, yEB002, yEB011, and yAM946, in which Pds5, Scs3, and Eco1 were fused to auxin-induced degron (AID); this enables their transient depletion through the supplementation of the growth medium with auxin. The AID proteins were undetectable by Western blot after supplementing the growth medium with 1 mM auxin (IAA) for 2 h (Fig EV3). The diffusion of Scs1-GFP in AID strains without auxin was similar to wild-type cells, suggesting that the AID has no detectable effect on the diffusion (Appendix Table S2).

Changes in Scs1-GFP in response to the deletion of WPL1 or auxin-induced depletion of Pds5, Scs3, and Eco1 were measured (Table 1 and Fig 3A–D). In WPL1Δ cells at S phase, the diffusion of Scs1 was twofold slower than wild-type cells, which is in agreement with the suggested destabilization activity of Wpl1, as cohesin becomes more stably bound to the chromatin when WPL1 is deleted [6,14,15]. Unexpectedly, the mobility of Scs1-GFP in WPL1Δ cells at G2 increased and was comparable to that of wild-type cells. However, in the M phase, the diffusion time of Scs1-GFP decreased, suggesting that Scs1-GFP remains associated with the chromatin in WPL1Δ cells. In contrast to the stabilization effect of Wpl1, the depletion of Pds5 increased the diffusion time at the S and G2

phases to ~4 ms, implying premature cohesin dissociation, which is in agreement with the role of Pds5 in cohesin maintenance [7,19].

Scs3 is essential for cohesin chromosomal residency and cohesion. Intriguingly, depletion of Scs3 resulted in slower diffusion of Scs1-GFP at all stages of the cell cycle. Under these conditions, the diffusion time of Scs1-GFP was ~17 ms. Eco1 acetylates Smc3 during the S phase and is essential for cohesin establishment. The diffusion of Scs1-GFP in cells following depletion of Eco1 at the S phase was 15.23 ms, similar to the diffusion after depletion of Scs3. At G2 phase, Scs1-GFP diffusion increased to 21.56 ms and decreased back to 9.2 ms at the M phase. Cohesin cannot be established in the absence of Scs3 or Eco1 [9,16,32–34]. Our data suggest that the association of Scs3 with cohesin induces a conformational change in the Smc1-Smc3-Scs1 trimer, which is important for chromatin binding. Similarly, the acetylation of Smc3 by Eco1 [17,18] may induce a conformational change that shifts cohesin to its cohesive mode.

FCS measurements were used to evaluate the concentration of the tagged proteins in cells, based on their fluorescence, as explained in the Materials and Methods section (Table 2). The concentration of Smc3-GFP, Scs3-GFP, and Scs1-GFP is similar during the S and G2 phase, as expected from their 1:1:1 ratio in cohesin. In M phase, the concentration of Scs1-GFP in the M phase is reduced to about 40–50% of its level at the S phase, most likely due to its cleavage and degradation.

#### Cohesin exists mostly in the monomeric state throughout the cell cycle

The possibility that cohesin complexes may exist as dimers or organized in other multimeric forms has been explored by PCH analysis of cells carrying Scs1-GFP. For control, we used yeast strains that express GFP or GFP-GFP to determine the molecular brightness of GFP monomers and dimers. Typical photon counting histograms of GFP and GFP-GFP dimers are shown in Fig 4A. As expected, the brightness of the GFP dimer was approximately twice that of the monomer. Having established the controls, cohesin stoichiometry was determined at different stages of the cell cycle (Fig 4B). Our results and analysis yielded only cohesin monomers; dimers or multimers were not observed in the S, G2, or M phase cells.

To examine the possible effect of cohesin regulators on stoichiometry, we performed PCH analysis in WPL1Δ, auxin-depleted Pds5, and Eco1 cells. Similar to the wild type, the monomeric form of cohesin in

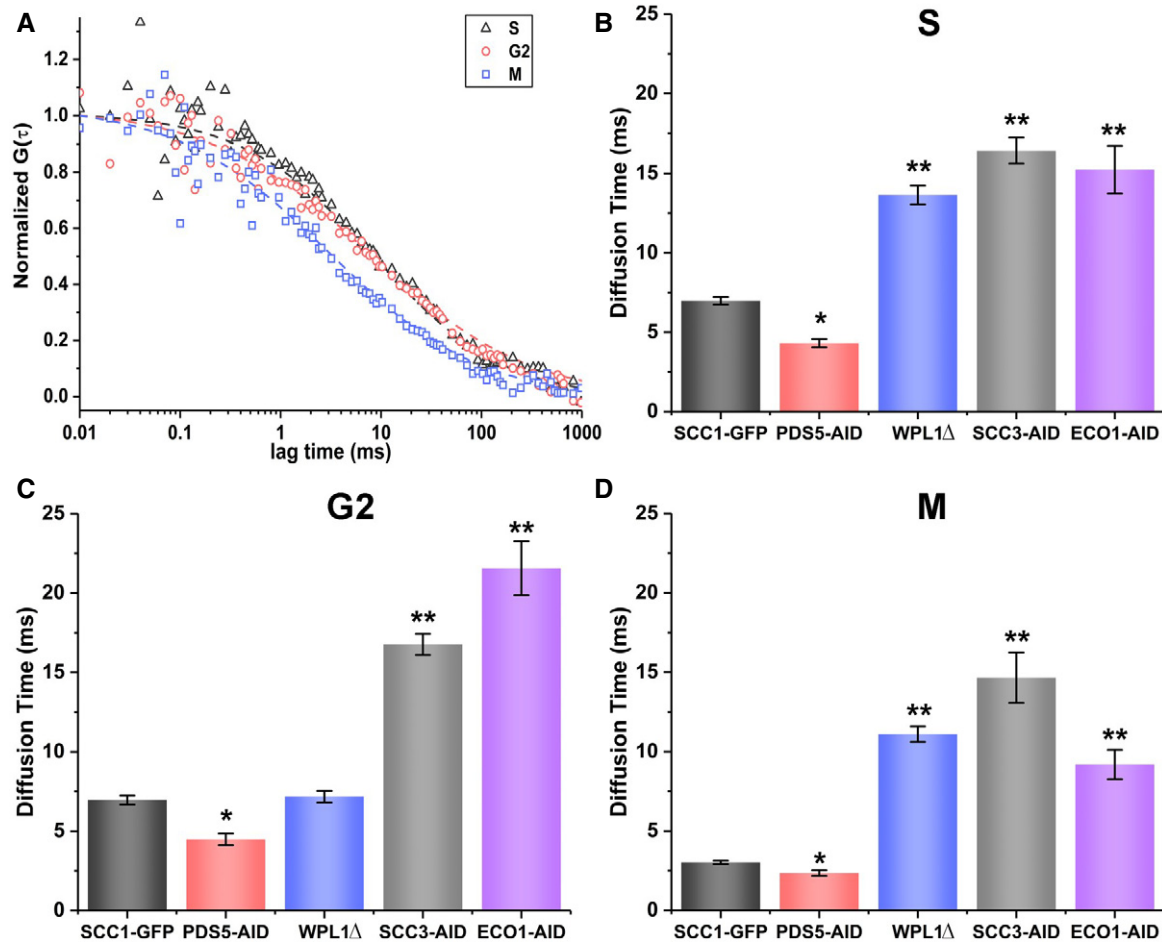


**Figure 3. The effect of subunit composition on cohesin diffusion time throughout the cell cycle.**

A Representative normalized FCS curve of Scc1-GFP at different cell cycle phases. Dotted lines indicate fitting of one-component anomalous diffusion models to the respective FCS curve.

B–D The diffusion times of Scc1-GFP at S phase (B), G2 phase (C), and M phase (D) were measured in strains yIO664 (wild-type) and yEB005 (WPL1Δ), and in auxin-depleted yEB002 (PDS5-AID), yAM085 (SCC3-AID), and yAM946 (ECO1-AID) cells. Data are shown as mean ± SEM from at least three independent experiments. \* $P < 10^{-5}$ ; \*\* $P < 10^{-13}$ .

these cells remained in this state (Fig 4B). The handcuff model of cohesin dimerization suggested that the dimerization of two cohesins is mediated by sharing a single subunit. To exclude the possibility that Scc1 is shared by two complexes, we repeated the PCH analysis with cells containing Scc3-GFP (Fig 4C). Only monomers were detected, suggesting that cohesin is a canonical monomer.

To eliminate the possibility that dimers are not detected due to the limitation of our experimental setup, we constructed two yeast strains yAM953 and yAP941 in which we tagged either SMC3 or SCC3 in addition to SCC1 with GFP. Therefore, we expected that if cohesin is indeed a monomer, the photon count from each cohesin complex will correspond to two GFP molecules. The handcuff model

**Table 2. Cellular concentration of cohesin subunits throughout the cell cycle.**

Subunit	Condition	G1	S	G2	M
Smc3-GFP		49.96 ± 4.06	166.64 ± 8.58	138.2 ± 3.53	128.1 ± 5.12
Scc3-GFP		78.78 ± 4.94	149.53 ± 10.56	151.26 ± 5.23	105.85 ± 10.85
Scc1-GFP		N/A	157.33 ± 3.67	108.0 ± 6.56	69.73 ± 2.0
Scc1-GFP	WPL1Δ	N/A	118.93 ± 4.8	109.83 ± 9.1	73.48 ± 10.93
Scc1-GFP	Pds5-AID	N/A	132.47 ± 5.86	151.28 ± 10.53	75.79 ± 12.48
Scc1-GFP	Scc3-AID	N/A	110.28 ± 7.46	92.88 ± 4.35	54.69 ± 7.43

Protein concentrations are in nM.

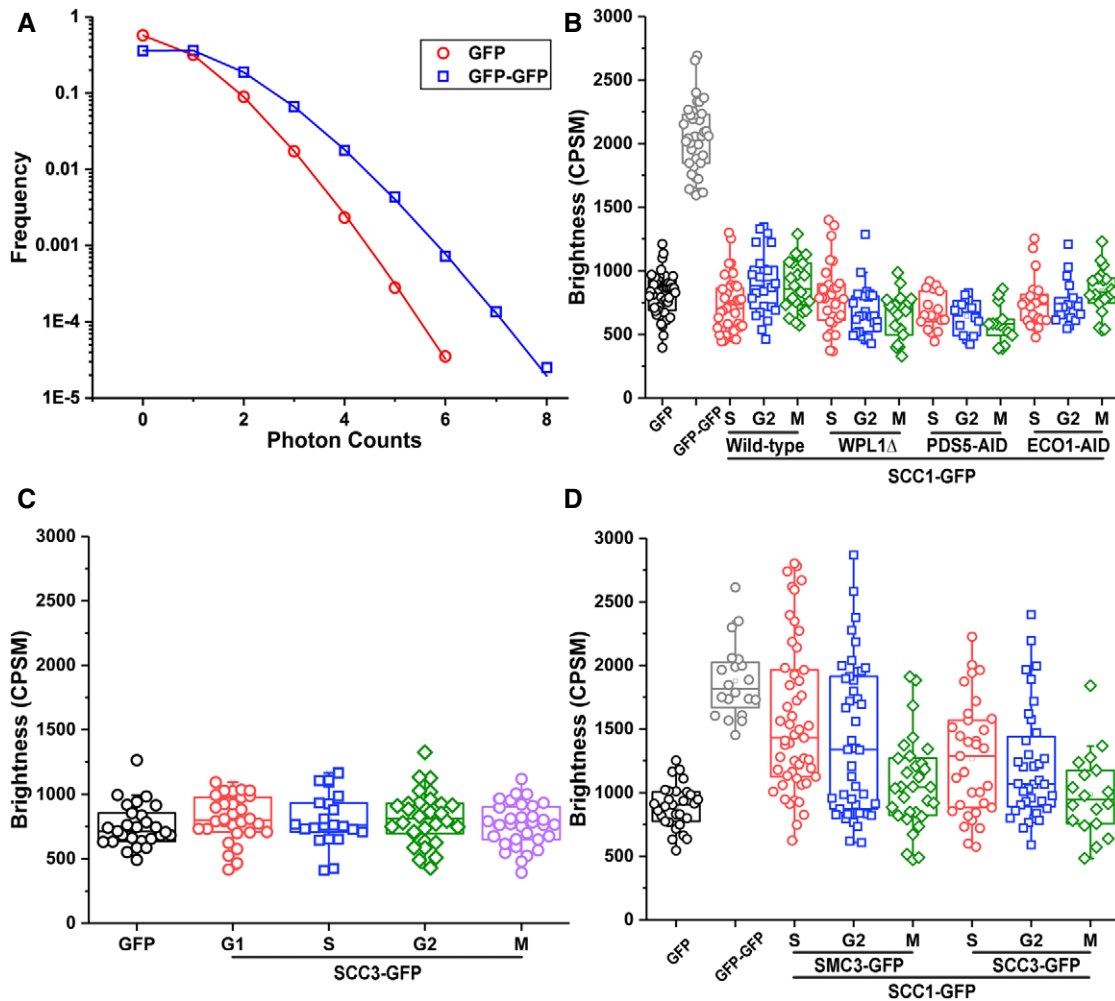


**Figure 4. Photon counting histogram (PCH) reveals a monomer form of cohesin.**

- A Typical fitted photon counting histograms of GFP and GFP-GFP in live yeast cells.
- B The molecular brightness of different GFP-tagged constructs was obtained with GFP monomer and GFP-GFP dimer as the brightness standard. Cells of strain yIO664 (SCC1-GFP) were analyzed throughout the cell cycle by PCH. To examine the effects of Wpl1, Pds5, and Eco1 on cohesin dimerization, the PCH analysis was repeated in strain yEB005 cells (SCC1-GFP WPL1 $\Delta$ ), strain yEB002 cells (SCC1-GFP PDS5-AID), and yAM946 (SCC1-GFP ECO1-AID) in which Pds5-AID/Eco1-AID was depleted with auxin.
- C PCH analysis of strain yAM085 (SMC3-GFP) throughout the cell cycle.
- D PCH analysis of strains yAM953 (SCC1-GFP SMC3-GFP) and yAP941 (SCC1-GFP SCC3-GFP) containing two GFP-tagged subunits. Data are shown as boxplot (+data overlap) with values of minimum, 5% percentile, 25% percentile, median, 75% percentile, maximum, and mean (center square marks) from at least three independent experiments.

suggests that cohesin dimers are formed by two tripartite Smc1-Smc3-Scc1 rings that are held by a single Scc3 subunit. In this case, PCH in cells carrying Scc1-GFP and Scc3-GFP is expected to correspond to three GFPs. The PCH results show only two GFPs per molecule (Fig 4D) and, therefore, fully support our conclusion on the monomeric state of cohesin in live cells.

Here, we analyzed the dynamics and stoichiometry of cohesin in live cells. We found changes in cohesin diffusion time that depend on both the cell cycle and subunit composition of the complex. These changes in cohesin diffusion may reflect interactions with chromatin and major conformational changes. In addition, we showed that cohesin complexes remain as monomers. No conclusive evidence of cohesin dimers or other multimers was noted.

These results provide new insight into cohesin dynamics in live cells.

The diffusion of proteins in live cells is affected by multiple non-exclusive factors that include molecular interactions, conformation, volume exclusion, and collision in the nucleus. Most importantly, cell cycle-dependent chromatin dynamics can also affect the local environment of chromatin density. All these possibilities should be kept in mind when interpreting FCS data from live cells. Considering these factors, the measured diffusion of cohesin subunits at different stages of the cell cycle is consistent with the current model of the cohesin activity cycle. We found that the diffusion time of Smc3 and Scc3 is lower in the G1 than the S phase of the cell cycle. In the G1 phase, Scc1 is not expressed, and

therefore, cohesin is not assembled. The slower diffusion of Smc3 compared with Scc3 suggests that Smc3 possibly exists in the dimerized form with Smc1, while Scc3 forms a subcomplex with Wpl1 and possibly Scc2/4 or Pds5. In the S and G2 phases, the diffusion times of both Smc3 and Scc3 are similar to that of Scc1 and most likely associated with the cohesin complex assembly and formation of stable cohesin–DNA complexes. In mitotic cells, Scc1 is cleaved by separase, and cohesin is fully released from chromosomes. At this stage, we noted a faster diffusion of Scc1 and Scc3. Surprisingly, Smc3 has a slower diffusion at M phase. This may be explained by transformation of the SMC proteins to a rod shape after Scc1 cleavage [5,13].

The effect of depleting cohesin regulatory subunit proteins on the diffusion of Scc1 was measured. The deletion of WPL1 resulted in slower Scc1 diffusion compared with the holocomplex in S and M phases. However, in G2 phase, the diffusion time of Scc1-GFP in WPL1Δ cells was found to be similar to the protein in wild-type cells. These results suggest that Wpl1 in yeast may play a role in cohesin loading and release but not to cohesion maintenance [15,35]. In mammalian cells, in the absence of Wpl1, cohesin is not released from the chromatin [6,8]. Our results suggest that Wpl1 plays a similar role in yeast. The depletion of Pds5 by the auxin degron system had an opposite effect on Scc1 diffusion and led to an acceleration of Scc1 movement, indicating premature cohesin release from the chromatin [7,19]. Surprisingly, the deletion of Scc3 and Eco1 led to a longer diffusion time of Scc1 in the S, G2, and M phases.

We and others have suggested that cohesin adopts a function-related conformation and can shift between conformations [36–38]. These conformations may include an open ring conformation and a compact structure such as rod or folded conformation. Both Scc3 and Eco1 are essential for cohesin tethering activity [16–18]. Based on these results, we suggest that the non-cohesive form of cohesin is open while the chromatin-bound complex is compact. The depletion of Scc3 inhibits the conformational change and stabilizes cohesin in an open conformation that is reflected by the longer diffusion time. Therefore, we predict that Scc3 is a key subunit that controls cohesin conformation. In the absence of Eco1, cohesin conformation at S phase is open, similar to conformation without Scc3. Eco1 depletion inhibits Smc3 acetylation and cohesion establishment. In turn, the complex maintains its open conformation throughout the cell cycle.

The mechanism of chromosome tethering is a long-standing debate. Biochemical evidence supports a monomeric ring model, while genetic evidence indicates cohesin dimerization. Our single-cell analysis of cohesin in live yeast cells identified monomers under all experimental conditions. Ours is also the first experiment to explore this mechanism in live cells. Furthermore, we showed that neither cell cycle nor cohesin auxiliary subunits induce multimerization of cohesin. In addition, the experiments in which two separate subunits were tagged with GFP strongly argue against the handcuff model in which Scc3 is shared by two Smc1-Smc3-Scc1 rings. Therefore, our results favor the model by which cohesin is active as a monomeric ring. However, we cannot completely rule out the possibility of a small fraction of cohesin present as dimers, or the existence of location-dependent dimerization as measured by ensemble characterization of cohesin subunits at the single-cell level, where only 10–30% of cohesin was found to be sufficient to support the

mitotic cohesion [39,40]. The discrepancy between the results obtained by different experimental approaches is yet to be settled.

## Materials and Methods

### Yeast strains and growth

The yeast strains used in this work are listed in Appendix Table S3. The strains were constructed using standard molecular and genetic methods. Cells were grown in YPD or SD medium, as indicated [9,38,41]. Auxin-induced degradation [42,43] was done as described in Ref. [9,38]. Protein depletion was validated by semi-quantitative growth assays on YPD plates, with and without auxin (IAA) (Sigma-Aldrich), and by Western blot with antibodies against V5 (Invitrogen) and tubulin (Abcam).

### Single-molecule fluorescence lifetime imaging system

Live yeast cell fluorescence fluctuation spectroscopy (FFS) and imaging were performed using the Alba Confocal Lifetime Imaging system (ISS, Inc.). The fluorescence lifetime imaging system is described elsewhere [44,45]. Briefly, a 488 nm picosecond pulsed laser was used to excite the GFP-tagged protein. The excitation beam was delivered to the sample stage through an apochromatic water immersion objective (60×, NA = 1.2, Olympus), and fluorescence was collected by the same objective. A 50-μm pinhole was employed to block off-focus photons, and the final signal was filtered by a band-pass filter (520/43, Chroma) before detecting by a photon avalanche photodiode detector (SPCM-AQRH-15, Excelitas). Photons were recorded using a time-correlated single-photon counting module in the time-tagged time-resolved mode (TTTR). Autocorrelation data were analyzed in VistaVision (ISS) and OriginPro.

### Fluorescence correlation spectroscopy in living yeast

Yeast cells were cultured with synthetic defined medium at 2% dextrose (Sigma), 6.7 g/l of yeast nitrogen base without amino acids (Sigma), and complete supplement mixture or amino acid drop out mixture as required (Formedium). Overnight yeast culture was diluted to O.D. ~0.1 to 0.2 and subcultured at 27°C in the dark. For live-cell measurements, around 1 ml of yeast cells (in mid-log phase) was pipetted on the 18-mm, no. 1.5H round coverslip (Azer Scientific) and maintained in an in-house 3D printed coverslip holder before transferring to a live-cell chamber (Tokai Hit, Japan) at 27°C. Coverslips were precoated with 0.1 mg/ml concanavalin A (Sigma) for 60 min, rinsed with molecular biology grade water (Corning), and stored in the dark at 4°C before use. The cell cycle stage was defined by morphology as follows: S phase, where cells show a tiny bud with undivided nuclei; G2 phase comprises of medium-budded cells with nuclei near the neck; and M phase is large-budded cells with nuclei GFP signals present in both mother and daughter cells (Fig EV1). G1 cell synchronization was achieved with alpha-factor mating pheromone (Zymo Research). M phase arrest was performed with nocodazole (Santa Cruz Biotechnology) [9,38,41].

FCS measurements were carried out using the Alba Fluorescence Lifetime Imaging system. Ten 10-s fluorescence trace measurements

were taken per cell with an average laser power of  $\sim 0.2 \mu\text{W}$  (measured at the back aperture of the objective) to minimize photobleaching effects in each segment of the data, and the data were averaged per cell for FCS analysis [46,47]. Cells were measured within 45 min after mounting on the coverslip [48]. FCS analysis is described elsewhere in our previous work [46,48,49]. For FCS measurement, the autocorrelation function  $G(t)$  is defined as follows:

$$G(\tau) = \frac{\langle \delta F(t) \cdot \delta F(t + \tau) \rangle}{\langle \delta F(t) \rangle^2} \quad (1)$$

Where  $\langle F \rangle$  is the average fluorescence intensity and  $\delta F(t) = F(t) - \langle F(t) \rangle$ .

For solution measurements,  $G(\tau)$  was fitted with:

$$G(\tau) = \frac{\gamma}{\langle N \rangle} \cdot \frac{1}{1 + \frac{\tau}{\tau_D}} \cdot \frac{1}{\sqrt{1 + \frac{1}{\kappa^2} \cdot \frac{\tau}{\tau_D}}} \quad (2)$$

where  $\kappa = \frac{z_0}{\omega_0}$  represents the structure parameter of the confocal profile.  $\tau_D$  is the characteristic diffusion time of fluorescence molecules, which reflects the transit dwell time in the effective detection volume.  $\kappa$  was calibrated using a known concentration of rhodamine 110 solution at the beginning of each experiment day.  $\langle N \rangle$  is the average number of fluorescent particles in the excitation–detection volume.  $\gamma$  is 0.3536 for 1-photon FCS under 488 nm excitation.

For yeast cell FCS experiments, the acquired  $G(\tau)$  was fitted with the standard equation for the free, 3D anomalous diffusion model:

$$G(\tau) = \frac{\gamma}{\langle N \rangle} \cdot \frac{1}{1 + \left(\frac{\tau}{\tau_D}\right)^\alpha} \cdot \frac{1}{\sqrt{1 + \frac{1}{\kappa^2} \cdot \left(\frac{\tau}{\tau_D}\right)^\alpha}} \quad (3)$$

where  $\alpha$  is the degree of anomalous behavior, and 0.5–0.8 indicates anomalous diffusion. Five hundred iterations of a Levenberg–Marquardt algorithm were employed for fitting both PCH and FCS data to minimize reduced chi-square. A globally reduced  $\chi^2 \sim 1$  was reached for the analysis.

The diffusion time  $\tau_D$  is related to the diffusion coefficient  $D$  by

$$\tau_D = \frac{\omega_0^2}{4D} \quad (4)$$

Cohesin dynamics is complex and involves multiple interacting partners such as cohesin–DNA, cohesin subunit interaction, and cohesin conformational change, among others in the nucleus environment where the presence of chromatin presence is an additional obstacle to diffusion. Distinguishing each diffusion component presents significant technical difficulty, and hence, we used the one-component anomalous diffusion model to quantify the overall “apparent” diffusion time of cohesin subunits during cell cycle progression. Anomalous diffusion model was used as fitting model because we did not observe distinct 2-component FCS curve in the experiments. A comparison of one- versus two-component analysis is shown in Fig EV4. No significant improvement in the fitting was achieved with the two-component model.

For PCH, the fundamental equation to determine molecular brightness is given by [50]:

$$\varepsilon = I_0^n \beta \eta_I \quad (5)$$

where  $\varepsilon$  is the brightness (counts per second per molecule, CPSM),  $\eta_I$  is the detection efficiency,  $I_0^n$  is the maximum excitation at the center of the detection volume for the one-photon system, and  $\beta$  is the excitation probability. The PCH algorithm for a 3D Gaussian confocal volume, which accounts for afterpulsing and dead-time effect, is provided by VistaVision software (ISS) according to the literature [51,52]. The histogram of detected photons with an integration time of 50  $\mu\text{s}$  was used for analysis. Laser intensity was set to the value determined by the intensity control unit in the Alba system with an electronically controlled neutral density filter wheel. Identical laser power was used in experiments with SCC1-GFP strains, and yeast cells expressing GFP and GFP-GFP were evaluated as standard control of monomer and dimer GFP brightness. Fluorescence intensity measurements of 3–10 s, without noticeable photodepletion, were used for analysis, and 3–5 measurements were grouped to determine the molecular brightness of a single cell.

**Expanded View** for this article is available online.

## Acknowledgements

We thank Vinny Guacci and Doug Koshland for providing yeast strains, and Ann L. Kirchmaier and Rong Li for providing PCH control yeast strains. W.L. thanks Jiji Chen and Brian D. Slaughter for helpful discussion on yeast FCS. W.L. thanks undergraduate students in J.I. Laboratory. We also thank members of the Onn Laboratory for their support. This work was supported by the Israel Science Foundation Grant 1099/16 (IO). JI thanks the W.M. Keck Foundation for the support.

## Author contributions

WL performed FCS and PCH and analyzed the results. EB, AP, and AM constructed yeast strains and validated protein expression and AID depletions. AP also performed microscopy and live-cell imaging. AM provided technical assistance and validated results. WL, EB, AP, and AM prepared the figures. JI and IO designed the study, supervised experiments, and wrote the paper with the input of all authors.

## Conflict of interest

The authors declare that they have no conflict of interest.

## References

- Onn I, Heidinger-Pauli JM, Guacci V, Unal E, Koshland DE (2008) Sister chromatid cohesion: a simple concept with a complex reality. *Annu Rev Cell Dev Biol* 24: 105–129
- Hassler M, Shaltiel IA, Haering CH (2018) Towards a unified model of SMC complex function. *Curr Biol* 28: R1266–R1281
- Uhlmann F (2016) SMC complexes: from DNA to chromosomes. *Nat Rev Mol Cell Biol* 17: 399–412
- van Ruiten MS, Rowland BD (2018) SMC complexes: universal DNA looping machines with distinct regulators. *Trends Genet* 34: 477–487
- Michaelis C, Ciosk R, Nasmyth K (1997) Cohesins: chromosomal proteins that prevent premature separation of sister chromatids. *Cell* 91: 35–45
- Gandhi R, Gillespie PJ, Hirano T (2006) Human Wapl is a cohesin-binding protein that promotes sister-chromatid resolution in mitotic prophase. *Curr Biol* 16: 2406–2417



7. Hartman T, Stead K, Koshland D, Guacci V (2000) Pds5p is an essential chromosomal protein required for both sister chromatid cohesion and condensation in *Saccharomyces cerevisiae*. *J Cell Biol* 151: 613–626
8. Kueng S, Hegemann B, Peters BH, Lipp JJ, Schleiffer A, Mechtler K, Peters JM (2006) Wapl controls the dynamic association of cohesin with chromatin. *Cell* 127: 955–967
9. Orgil O, Matityahu A, Eng T, Guacci V, Koshland D, Onn I (2015) A conserved domain in the scc3 subunit of cohesin mediates the interaction with both mcd1 and the cohesin loader complex. *PLoS Genet* 11: e1005036
10. Stead K, Aguilar C, Hartman T, Drexel M, Meluh P, Guacci V (2003) Pds5p regulates the maintenance of sister chromatid cohesion and is sumoylated to promote the dissolution of cohesion. *J Cell Biol* 163: 729–741
11. Uhlmann F, Lottspeich F, Nasmyth K (1999) Sister-chromatid separation at anaphase onset is promoted by cleavage of the cohesin subunit Scc1. *Nature* 400: 37–42
12. Rao H, Uhlmann F, Nasmyth K, Varshavsky A (2001) Degradation of a cohesin subunit by the N-end rule pathway is essential for chromosome stability. *Nature* 410: 955–959
13. Guacci V, Koshland D, Strunnikov A (1997) A direct link between sister chromatid cohesion and chromosome condensation revealed through the analysis of MCD1 in *Saccharomyces cerevisiae*. *Cell* 91: 47–57
14. Sutani T, Kawaguchi T, Kanno R, Itoh T, Shirahige K (2009) Budding yeast Wpl1(Rad61)-Pds5 complex counteracts sister chromatid cohesion-establishing reaction. *Curr Biol* 19: 492–497
15. Lopez-Serra L, Lengronne A, Borges V, Kelly G, Uhlmann F (2013) Budding yeast Wapl controls sister chromatid cohesion maintenance and chromosome condensation. *Curr Biol* 23: 64–69
16. Ivanov D, Schleiffer A, Eisenhaber F, Mechtler K, Haering CH, Nasmyth K (2002) Eco1 is a novel acetyltransferase that can acetylate proteins involved in cohesion. *Curr Biol* 12: 323–328
17. Rolef Ben-Shahar T, Heeger S, Lehane C, East P, Flynn H, Skehel M, Uhlmann F (2008) Eco1-dependent cohesin acetylation during establishment of sister chromatid cohesion. *Science* 321: 563–566
18. Unal E, Heidingen-Pauli JM, Kim W, Guacci V, Onn I, Gygi SP, Koshland DE (2008) A molecular determinant for the establishment of sister chromatid cohesion. *Science* 321: 566–569
19. Panizza S, Tanaka T, Hochwagen A, Eisenhaber F, Nasmyth K (2000) Pds5 cooperates with cohesin in maintaining sister chromatid cohesion. *Curr Biol* 10: 1557–1564
20. Yanagida M (2000) Cell cycle mechanisms of sister chromatid separation; roles of Cut1/separin and Cut2/securin. *Genes Cells* 5: 1–8
21. Ivanov D, Nasmyth K (2007) A physical assay for sister chromatid cohesion *in vitro*. *Mol Cell* 27: 300–310
22. Mc Intyre J, Muller EG, Weitzer S, Snyderman BE, Davis TN, Uhlmann F (2007) *In vivo* analysis of cohesin architecture using FRET in the budding yeast *Saccharomyces cerevisiae*. *EMBO J* 26: 3783–3793
23. Minamino M, Higashi TL, Bouchoux C, Uhlmann F (2018) Topological *in vitro* loading of the budding yeast cohesin ring onto DNA. *Life Sci Alliance* 1. <https://doi.org/10.26508/lsa.201800143>
24. Weitzer S, Lehane C, Uhlmann F (2003) A model for ATP hydrolysis-dependent binding of cohesin to DNA. *Curr Biol* 13: 1930–1940
25. Eng T, Guacci V, Koshland D (2014) ROCC, a conserved region in cohesin's Mcd1 subunit, is essential for the proper regulation of the maintenance of cohesion and establishment of condensation. *Mol Biol Cell* 25: 2351–2364
26. Eng T, Guacci V, Koshland D (2015) Interallelic complementation provides functional evidence for cohesin-cohesin interactions on DNA. *Mol Biol Cell* 26: 4224–4235
27. Huang CE, Milutinovich M, Koshland D (2005) Rings, bracelet or snaps: fashionable alternatives for Smc complexes. *Philos Trans R Soc Lond B Biol Sci* 360: 537–542
28. Zhang N, Kuznetsov SG, Sharan SK, Li K, Rao PH, Pati D (2008) A handcuff model for the cohesin complex. *J Cell Biol* 183: 1019–1031
29. Ma Y, Kanakousaki K, Buttitta L (2015) How the cell cycle impacts chromatin architecture and influences cell fate. *Front Genet* 6: 19
30. Yamin K, Assa M, Matityahu A, Onn I (2019) Analyzing chromosome condensation in yeast by second-harmonic generation microscopy. *Curr Genet*. <https://doi.org/10.1007/s00294-019-01034-1>
31. Anderson DE, Losada A, Erickson HP, Hirano T (2002) Condensin and cohesin display different arm conformations with characteristic hinge angles. *J Cell Biol* 156: 419–424
32. Haering CH, Lowe J, Hochwagen A, Nasmyth K (2002) Molecular architecture of SMC proteins and the yeast cohesin complex. *Mol Cell* 9: 773–788
33. Onn I, Guacci V, Koshland DE (2009) The zinc finger of Eco1 enhances its acetyltransferase activity during sister chromatid cohesion. *Nucleic Acids Res* 37: 6126–6134
34. Toth A, Ciosk R, Uhlmann F, Galova M, Schleiffer A, Nasmyth K (1999) Yeast cohesin complex requires a conserved protein, Eco1p(Ctf7), to establish cohesion between sister chromatids during DNA replication. *Genes Dev* 13: 320–333
35. Srinivasan M, Petela NJ, Scheinost JC, Collier J, Voulgaris M, M BR, Beckouet F, Hu B, Nasmyth KA (2019) Scc2 counteracts a Wapl-independent mechanism that releases cohesin from chromosomes during G1. *Elife* 8: e44736
36. Kulemzina I, Ang K, Zhao X, Teh JT, Verma V, Suranthran S, Chavda AP, Huber RG, Eisenhaber B, Eisenhaber F et al (2016) A reversible association between Smc coiled coils is regulated by lysine acetylation and is required for cohesin association with the DNA. *Mol Cell* 63: 1044–1054
37. Matityahu A, Onn I (2018) A new twist in the coil: functions of the coiled-coil domain of structural maintenance of chromosome (SMC) proteins. *Curr Genet* 64: 109–116
38. Orgil O, Mor H, Matityahu A, Onn I (2016) Identification of a region in the coiled-coil domain of Smc3 that is essential for cohesin activity. *Nucleic Acids Res* 44: 6309–6317
39. Heidingen-Pauli JM, Mert O, Davenport C, Guacci V, Koshland D (2010) Systematic reduction of cohesin differentially affects chromosome segregation, condensation, and DNA repair. *Curr Biol* 20: 957–963
40. Zhang J, Shi X, Li Y, Kim BJ, Jia J, Huang Z, Yang T, Fu X, Jung SY, Wang Y et al (2008) Acetylation of Smc3 by Eco1 is required for S phase sister chromatid cohesion in both human and yeast. *Mol Cell* 31: 143–151
41. Shwartz M, Matityahu A, Onn I (2016) Identification of functional domains in the cohesin loader subunit Scc4 by a random insertion/dominant negative screen. *G3* 6: 2655–2663
42. Morawska M, Ulrich HD (2013) An expanded tool kit for the auxin-inducible degron system in budding yeast. *Yeast* 30: 341–351
43. Nishimura K, Fukagawa T, Takisawa H, Kakimoto T, Kanemaki M (2009) An auxin-based degron system for the rapid depletion of proteins in nonplant cells. *Nat Methods* 6: 917–922
44. Kuang L, Damayanti NP, Jiang C, Fei X, Liu W, Narayanan N, Irudayaraj J, Campanella O, Deng M (2019) Bioinspired glycosaminoglycan hydrogels via click chemistry for 3D dynamic cell encapsulation. *J Appl Polym Sci* 136: 47212
45. Liu W, Cui Y, Ren W, Irudayaraj J (2019) Epigenetic biomarker screening by FLIM-FRET for combination therapy in ER+ breast cancer. *Clin Epigenet* 11: 16

46. Cui Y, Irudayaraj J (2015) Dissecting the behavior and function of MBD3 in DNA methylation homeostasis by single-molecule spectroscopy and microscopy. *Nucleic Acids Res* 43: 3046–3055
47. Pack C-G, Yukii H, Toh-e A, Kudo T, Tsuchiya H, Kaiho A, Sakata E, Murata S, Yokosawa H, Sako Y et al (2014) Quantitative live-cell imaging reveals spatio-temporal dynamics and cytoplasmic assembly of the 26S proteasome. *Nat Commun* 5: 3396
48. Chen J, Miller A, Kirchmaier AL, Irudayaraj JMK (2012) Single-molecule tools elucidate H2AZ nucleosome composition. *J Cell Sci* 125: 2954–2964
49. Cui Y, Cho I-H, Chowdhury B, Irudayaraj J (2013) Real-time dynamics of methyl-CpG-binding domain protein 3 and its role in DNA demethylation by fluorescence correlation spectroscopy. *Epigenetics* 8: 1089–1100
50. Chen Y, Muller JD, So PT, Gratton E (1999) The photon counting histogram in fluorescence fluctuation spectroscopy. *Biophys J* 77: 553–567
51. Chen Y, Wei L-N, Müller JD (2003) Probing protein oligomerization in living cells with fluorescence fluctuation spectroscopy. *Proc Natl Acad Sci USA* 100: 15492
52. Hillelshiem LN, Müller JD (2003) The photon counting histogram in fluorescence fluctuation spectroscopy with non-ideal photodetectors. *Biophys J* 85: 1948–1958